

This article was downloaded by:

On: 15 January 2011

Access details: *Access Details: Free Access*

Publisher *Taylor & Francis*

Informa Ltd Registered in England and Wales Registered Number: 1072954 Registered office: Mortimer House, 37-41 Mortimer Street, London W1T 3JH, UK



Comments on Inorganic Chemistry

Publication details, including instructions for authors and subscription information:

<http://www.informaworld.com/smpp/title~content=t713455155>

The Use of X-Ray Absorption Spectroscopy for Detection of Metal-Metal Interactions. Application to Copper-Containing Enzymes

Robert A. Scott^a; Marly K. Eidsness^a

^a Departments of Chemistry and Biochemistry and Center for Metalloenzyme Studies, University of Georgia, Athens, Georgia

To cite this Article Scott, Robert A. and Eidsness, Marly K.(1988) 'The Use of X-Ray Absorption Spectroscopy for Detection of Metal-Metal Interactions. Application to Copper-Containing Enzymes', *Comments on Inorganic Chemistry*, 7: 5, 235 – 267

To link to this Article: DOI: 10.1080/02603598808072311

URL: <http://dx.doi.org/10.1080/02603598808072311>

PLEASE SCROLL DOWN FOR ARTICLE

Full terms and conditions of use: <http://www.informaworld.com/terms-and-conditions-of-access.pdf>

This article may be used for research, teaching and private study purposes. Any substantial or systematic reproduction, re-distribution, re-selling, loan or sub-licensing, systematic supply or distribution in any form to anyone is expressly forbidden.

The publisher does not give any warranty express or implied or make any representation that the contents will be complete or accurate or up to date. The accuracy of any instructions, formulae and drug doses should be independently verified with primary sources. The publisher shall not be liable for any loss, actions, claims, proceedings, demand or costs or damages whatsoever or howsoever caused arising directly or indirectly in connection with or arising out of the use of this material.

The Use of X-Ray Absorption Spectroscopy for Detection of Metal–Metal Interactions. Application to Copper-Containing Enzymes

ROBERT A. SCOTT and MARLY K. EIDSNES

*Departments of Chemistry and Biochemistry and
Center for Metalloenzyme Studies,
University of Georgia,
Athens, Georgia 30602*

The use of the extended x-ray absorption fine structure (EXAFS) technique for the identification of metal–metal distances in biomacromolecules is discussed. The Cu EXAFS data for a number of structurally characterized copper-containing binuclear complexes are analyzed to determine the viability of detecting a Cu···M (M = Cu, Fe) scattering interaction at ~ 3 Å in the presence of Cu···C interactions at approximately the same distance (deriving from the outer-shell atoms of heterocyclic ligands). The techniques developed are then applied to the oxidized and reduced forms of the copper-containing enzyme dopamine β -hydroxylase. Although in principle the EXAFS technique has the ability to distinguish C from M scatterers, based on differences in the backscattering amplitude and phase, in the absence of *a priori* knowledge of the distribution of C atoms about the Cu site, often no unambiguous determination of the presence or absence of a Cu···M interaction can be made. It is suggested that caution be used in attempting to assign Cu···M distances based on the analysis of outer-shell Fourier-transform peaks.

Key Words: EXAFS, metalloenzymes, binuclear sites, metal–metal distance, active site structure

The extended x-ray absorption fine structure (EXAFS) technique has proven extremely useful in directly determining the local coordination environment of a selected element (usually a metal) in

Comments Inorg. Chem.

1988, Vol. 7, No. 5, pp. 235–267

Reprints available directly from the publisher

Photocopying permitted by license only

© 1988 Gordon and Breach,
Science Publishers, Inc.
Printed in Great Britain

amorphous samples. One important application of this technique is in examining active site structures of metallobiomolecules and a number of reviews of recent progress in this field are available.¹⁻⁴ Although EXAFS is often used to examine only the relatively low atomic number atoms directly coordinated to the metal, the photoelectron scattering that is responsible for the EXAFS is also observed from atoms in the "outer coordination spheres" (i.e., atoms that are not directly bonded to the metal). In particular, the presence of a heavy atom (e.g., another metal) in the vicinity of the absorbing atom should give rise to enhanced photoelectron scattering and, for this reason, it is often said that the EXAFS technique is well-suited to the determination of metal-metal interactions (e.g., in multinuclear sites of metalloenzymes).

In fact, the use of EXAFS in determining a metal-metal distance (thus confirming the existence of a multinuclear site) has experienced limited success. The utility of EXAFS in this regard may be evaluated by its ability to identify the presence of a metal scatterer in the vicinity of the absorbing metal atom in the *absence* of independent evidence for the existence of a multinuclear site. The Fe EXAFS of Fe-S cluster-containing proteins can hardly be considered an appropriate test, since much independent information had already led to a very good approximate structure for such clusters. In addition, Fe-S clusters represent a *best-case* example of metal-metal scattering, since the relatively rigid nature of these clusters holds the Fe atoms close together (~ 2.7 Å) yielding strong Fe...Fe scattering. Fe EXAFS did yield a reasonable distance for the Fe...Fe separation in various forms of hemerythrin,⁵⁻⁷ but it was already clear that the binuclear site was present; only the precise metrical details were missing.

A better test case involves the Cu EXAFS of the deoxy form of hemocyanin. The existence of a binuclear site in the oxy derivative was required to explain the magnetism of the site, but at the time of two independent EXAFS investigations, nothing was known about the structure in the deoxy derivative. One group of investigators calculated a Cu(I)...Cu(I) distance of 3.4 Å,⁸ while the other group claimed that the two Cu(I)'s were >4 Å apart.^{9,10} A recent deoxyhemocyanin crystal structure seems to support a shorter Cu(I)...Cu(I) distance.¹¹ A similar situation exists with the Cu...Fe binuclear O₂-interaction site of cytochrome c oxidase. One group of investigators calculates a Cu_B...Fe_{a3} distance of ~ 3.0 Å,¹² while

the other group reports a value of ~ 3.8 Å.¹³ Although, in this particular case, there is still some question about whether real structural differences among various enzyme preparations are responsible for the contradictory results, it is disconcerting that the EXAFS technique has not yielded more definitive answers.

The seemingly poor performance of the EXAFS technique in detecting metal–metal scattering is *not* related to an inherent flaw in the ability of EXAFS to identify scattering atom types (i.e., atomic numbers, Z). It is a direct result of the presence of other scattering atoms at radial distances near the metal–metal distance. In an ideal world, the absorbing metal is coordinated by low- Z atoms at distances of ~ 2 Å and the potential second metal is some longer distance away (perhaps 3–4 Å). The EXAFS Fourier transform (FT) would show two peaks, the second one of which would exhibit scattering characteristics (amplitude envelope shape, phase) of only the second metal, which would then be easily identifiable. In the real world, the ubiquity of histidine imidazoles as metal ligands places shells of C and N atoms at distances of ~ 3 and ~ 4 Å from the absorbing metal which yield scattering that combines and interferes with scattering from a second metal in that distance range. Other biological ligands (e.g., cysteine, methionine, tyrosine, etc.) also contribute such “second shell” C atoms in this region. Discrete FT peaks are often still observed but the question changes from “Does this FT peak have the scattering characteristics of a metal?” to “Can this FT peak be simulated by a distribution of C atoms or does the inclusion of a metal scatterer *significantly* improve this simulation?” The presence of the word “significantly” in this latter question makes the assignment of a metal scatterer considerably more subjective.

In order to determine the true capabilities of the EXAFS technique in detecting metal–metal interactions, we describe here Cu EXAFS of structurally characterized Cu compounds containing only “second-shell” C atoms or additionally containing a second metal (either Fe or Cu). Three different methods are explored to test our ability to detect Cu \cdots M interactions. These test cases serve to illustrate the difficulties involved in deciding whether a metal–metal interaction exists based on outer-shell EXAFS scattering. As a biological example, this analysis is then applied to the oxidized and reduced forms of the Cu-containing enzyme, dopamine β -hydroxylase.

DATA ANALYSIS

Our usual data reduction and analysis techniques were used.¹ The analysis makes use of the plane-wave, single-scattering EXAFS expression (Eq. (1)), where the EXAFS quantity χ is described as a function of photoelectron wave vector \mathbf{k} . N_s is the number of identical scatterers in a particular shell, R_{as} is the absorber–scatterer distance, and σ_{as} is the rms deviation in distance. The scattering characteristics of a particular shell of atoms are given by a scattering amplitude $[B_s|f_s(\pi, \mathbf{k})|]$ and phase $[\alpha_{as}(\mathbf{k})]$. Differences in these quantities allow one to distinguish a low- Z scatterer (e.g., C) from a high- Z scatterer (e.g., a metal).

$$\chi(\mathbf{k}) = \sum_s \frac{B_s N_s |f_s(\pi, \mathbf{k})|}{k R_{as}^2} \exp(-2\sigma_{as}^2 k^2) \sin[2kR_{as} + \alpha_{as}(\mathbf{k})] \quad (1)$$

For example, theoretical Cu–C and Cu–Cu backscattering amplitudes and phases are compared in Fig. 1. In Fig. 1a, the theoretical scattering functions calculated by Teo and Lee¹⁴ were used to compare the simulated Cu EXAFS (weighted by k^3) of a shell of four carbons with that from a shell of one copper (both at a distance of 3.0 Å). As expected, backscattering from a heavy scatterer (Cu) results in a $k^3\chi(\mathbf{k})$ contribution that maximizes at a significantly higher k than backscattering from a light scatterer (C). This difference in backscattering amplitude envelope shape can be exploited to distinguish Cu···C and Cu···Cu (or other Cu···M) scattering. A convenient method for making this comparison of the shape of these envelopes (Method 1, *vide infra*) is to compare the relative height of FT peaks generated by Fourier transformation with k^n weighting of $\chi(\mathbf{k})$ (varying n). In Fig. 1b, the theoretical phases $[\alpha_{as}(\mathbf{k})]$ are compared for Cu–C and Cu–Cu backscattering. Although it is not clear whether the phase difference observed in Fig. 1b is sufficient to allow a distinction to be made, in principle phase comparison is another method (Method 2, *vide infra*) that could be used to distinguish heavy and light atom scattering. Of course, standard EXAFS curve-fitting techniques rely on differences in both backscattering amplitude and phase to simulate the EXAFS contribution from Cu···C or Cu···M interactions. Method 3 consists of using standard curve-fitting optimizations to

determine the necessity of a Cu...M component for properly simulating a filtered outer-shell FT peak.

Method 1: k^n -Weighted Fourier Transformation. It is common practice to use $k^n\chi(k)$ ($n = 2,3$) instead of just $\chi(k)$ as the function to be Fourier transformed in EXAFS analysis. The k^n weighting function highlights the EXAFS oscillations at high k (relative to those at low k), thus effectively serving as a resolution enhancement function in the Fourier transform. An EXAFS contribution from Cu...M scattering maximizing at higher k is expected to yield an FT peak, the height of which is more strongly dependent on n than one resulting from Cu...C scattering (see Fig. 1a). For example, comparing FTs in which the weighting functions k^3 , k^4 , k^5 are used should yield a Cu...Cu FT peak with increasing height as n increases from 3 to 5, but a Cu...C FT peak height that is not dependent on n . One problem with such an approach is that the k^n weighting function affects the overall size of FT peaks and so some scaling must be done to directly compare the peaks. Often, FT peak heights for outer-shell peaks are compared relative to the height of the first-shell FT peak. This may not be the best scaling procedure, since the first-shell FT peak is also expected to have some k^n dependence which may vary from one compound to another. An alternative scaling procedure (used here) is to correct for the k^n weighting function by choosing some k_0 (independent of the compound being examined) and dividing the FT magnitudes by k_0^n before comparing them. The choice of k_0 is somewhat arbitrary, but we find that $k_0 = 8 \text{ \AA}^{-1}$ gives the desired effect. For example, Fig. 2 shows k^n -weighted FT comparisons for the simulated data in Fig. 1. For Cu...C only (solid line in Fig. 1a), Fig. 2a shows no monotonic trend of k^n -weighted FT peak height with n . However, for Cu...Cu (dashed line in Fig. 1a), Fig. 2b shows the expected monotonic increase of k^n -weighted FT peak height with increasing n . Unfortunately, if a real-world situation of a combination of Cu...C and Cu...Cu interactions at similar distances is simulated, then the EXAFS may lose most of the distinguishing backscattering amplitude envelope shape (Fig. 1c) and, consequently, the monotonic dependence of k^n -weighted FT peak height on n (Fig. 2c). This behavior will of course depend on the actual distances, coordination numbers, and Debye–Waller factors for the Cu...C and Cu...Cu shells, but we should at least expect

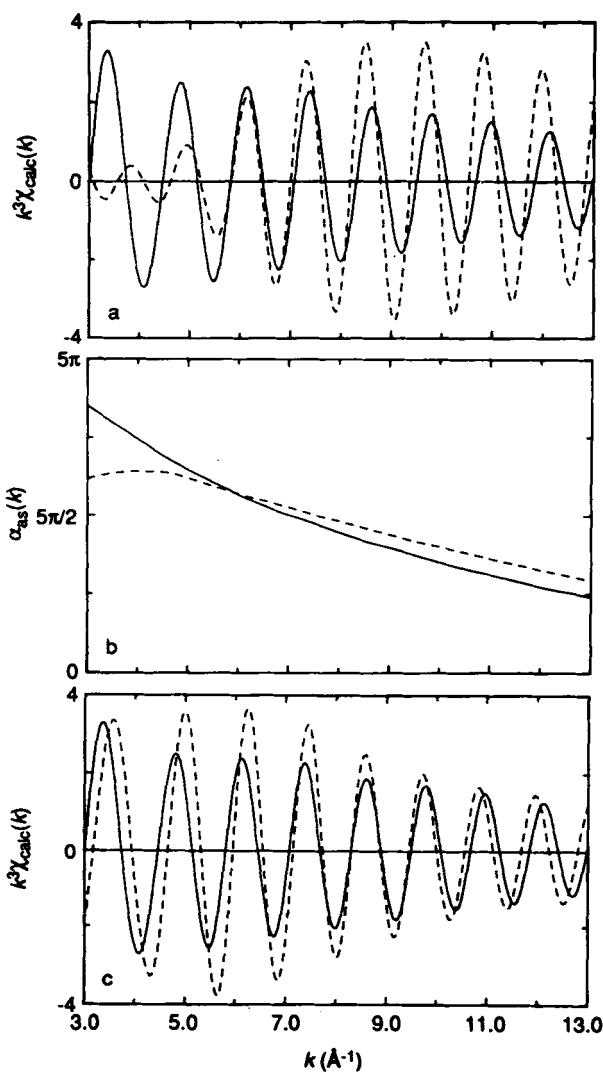


FIGURE 1 Simulated Cu EXAFS using theoretical Cu-C and Cu-Cu scattering functions. (a) Calculated scattering from 4C @ 3.0 Å (—) and 1 Cu @ 3.0 Å (---). (b) Theoretical phases [$\alpha_{\text{as}}(k)$, see Eq. (1)] for Cu-C (—) and Cu-Cu (---) scattering. (c) Calculated scattering from 4 C @ 3.0 Å (—) and 1 Cu @ 3.0 Å + 4 C @ 2.9 Å (---). In (a) and (c), all σ_{as} values were chosen as 0.05 Å.

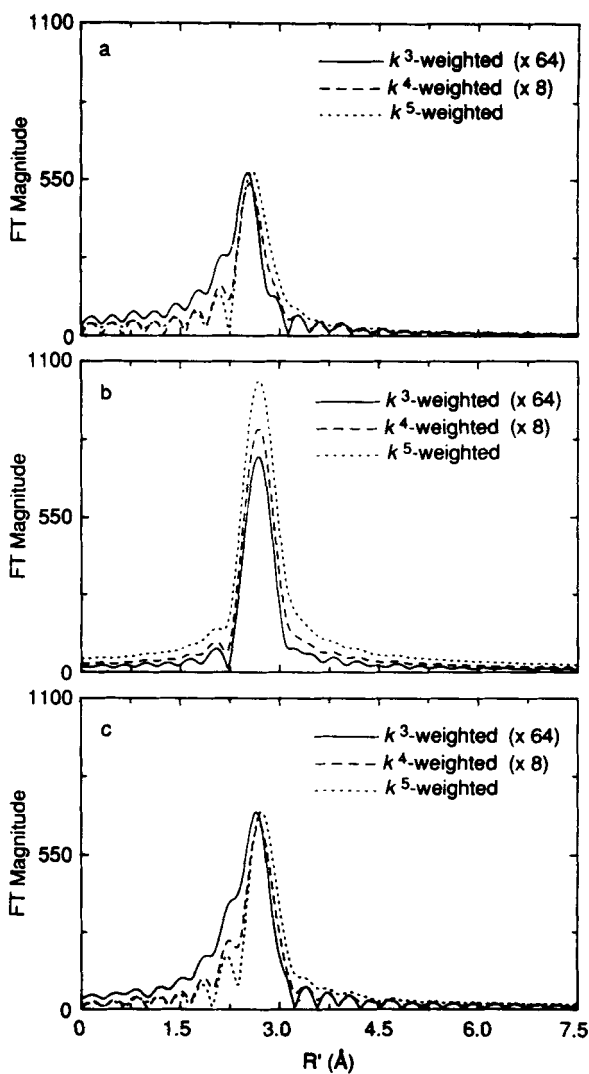


FIGURE 2 Fourier transforms (FTs) of simulated Cu EXAFS in Fig. 1. All FT ranges are $k = 3\text{--}13 \text{ \AA}^{-1}$. (a) k^n -weighted FTs ($n = 3\text{--}5$) of solid line in Fig. 1a, 4 C @ 3.0 \AA . (b) k^n -weighted FTs ($n = 3\text{--}5$) of dashed line in Fig. 1a, 1 Cu @ 3.0 \AA . (c) k^n -weighted FTs ($n = 3\text{--}5$) of dashed line in Fig. 1c, 4 C @ 2.9 \AA + 1 Cu @ 3.0 \AA .

difficulty in using this method to *confidently* detect Cu...M interactions in the presence of Cu...C interactions.

Method 2: Phase Comparison. The phase shift $\alpha_{as}(\mathbf{k})$ [see Eq. (1)] should be different for Cu...Cu and Cu...C backscattering. For a particular outer-shell FT peak, the effective phase shift may be extracted by complex Fourier back-transformation,^{1,15} given a knowledge of R_{as} [so that the $2\mathbf{k}R_{as}$ term may be removed from the sine argument in Eq. (1)]. In practice, one makes a comparison between the phase shift extracted from a FT peak from a (model) compound known to contain only Cu...C backscattering and the phase shift of a FT peak being tested for the presence of Cu...M scattering. This comparison should be restricted to FT peaks occurring at the same R' , using the R_{as} from the model for the phase shift extractions in both cases. Observation of a significant difference between the extracted phase shift of the unknown and model is then taken as evidence that some scatterer other than C (or N, O) is contributing to the FT peak in question. Determination of what is a *significant* difference may be accomplished by comparing the phase shifts of a number of model compounds with only Cu...C backscattering at the distance being examined.

Method 3: Curve Fitting. This method takes advantage of the differences in both backscattering amplitude and backscattering phase components for Cu...M versus Cu...C scattering. It is more difficult to apply because it requires quantitative knowledge of the actual backscattering functions for Cu...C and Cu...M. (The other methods simply depend on observation of qualitative differences in either amplitude or phase.) The theoretical scattering functions of Teo and Lee¹⁴ cannot be depended upon *a priori*, but may be useful in connection with a FABM-like approach,^{16,17} in which structurally characterized compounds are used to extract scale factors [B_C and B_M , see Eq. (1)] and ΔE_0 values [$\Delta E_0(C)$ and $\Delta E_0(M)$] for Cu...C and Cu...M backscattering. This is substantially more difficult for outer-shell (compared to first-shell) scattering, since a significant amount of disorder in Cu...C distances is common and since Cu...M scattering is never observed (in a relevant model) in the absence of Cu...C interference.

Given a good set of backscattering functions for Cu...C and Cu...M, the curve-fitting approach usually involves Fourier filter-

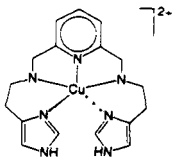
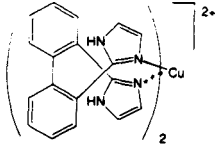
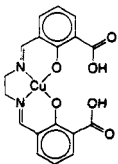
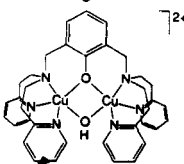
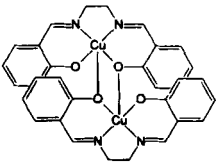
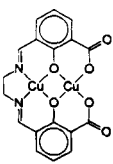
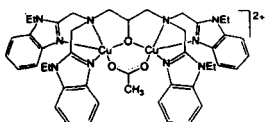
ing of the FT peak in question, followed by 2- (or 3-) shell curve fitting of the resultant filtered EXAFS data. For a copper site of unknown structure, it is reasonable to expect disorder in Cu...C outer-shell distances (e.g., from tilted imidazoles, or other outer-shell carbons in addition to imidazoles), so that a typical comparison may be between a two-shell Cu...C, Cu...C' fit and a two-shell Cu...C, Cu...M fit. The Cu...C, Cu...M fit must be judged significantly better in order to claim identification of a Cu...M interaction.

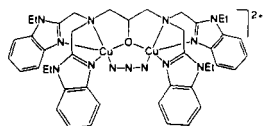
RESULTS AND DISCUSSION

Cu EXAFS data from a number of structurally characterized Cu mononuclear and Cu-M (M = Cu, Fe) binuclear compounds have been analyzed to test the ability of the three methods described above to identify Cu-M scattering. All of these compounds (Table I) exhibit first coordination spheres of N-, O-, or S-containing ligands and many have imidazole or imidazole-like ligands making them reasonable models for scattering that might be observed in a metalloenzyme copper active site.

Method 1. A particularly useful FT comparison is the homologous series of Cu, Cu-Cu, and Cu-Fe derivatives of the [(fsa)₂en] ligand shown in Fig. 3. Comparing first only the k^3 -weighted FTs (solid lines in Fig. 3), the mononuclear compound (C3, Fig. 3b) exhibits an unsymmetrical peak at $R' \approx 2.6$ Å due to scattering from a disordered set of carbons in the ligand. This FT peak is enhanced (relative to the first-shell FT peak) in the Cu-Cu binuclear derivative (CC3, Fig. 3a), attributable to the additional presence of Cu...Cu scattering (the Cu...Cu distance is 2.94 Å²³). In contrast, the Cu-Fe binuclear derivative (CF3, Fig. 3c) exhibits a *much reduced* intensity of the FT peak at $R' \approx 2.7$ Å (as well as enhanced FT intensity at $R' \approx 2.2$ Å). Since the structure of the Cu-Fe derivative²⁰ confirms the same set of outer-shell carbons as in the other derivatives and a similar Cu...Fe distance of 3.03 Å, the explanation for the reduced FT intensity must involve destructive interference between Cu...Fe and Cu...C backscattering components. Thus, the presence of a Cu...Fe interaction at ~ 3.0 Å *may* be almost completely masked by the presence of Cu...C interactions.

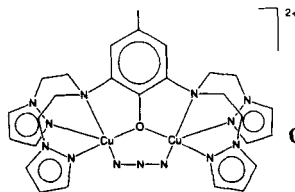
TABLE I
Copper compounds used in this work

Structure	No.	Name	Reference ^a
	C1	$[\text{Cu}(\text{imidH})_2\text{DAP}]^{2+}$	18
	C2	$\{\text{Cu}[2,2'-(\text{imid})_2\text{biphenyl}]\}_2^{2+}$	19
	C3	$\text{CuH}_2[(\text{fsa})_2\text{en}]$	20
	CC1	$[\text{Cu}_2(\text{L}')(\text{OH})]^{2+}$, IIIB	21
	CC2	$[\text{Cu}(\text{salen})]_2$	22
	CC3	$\text{Cu}_2[(\text{fsa})_2\text{en}]$	23
	CC4	$[\text{Cu}_2(\text{L-Et})(\text{OAc})]^{2+}$	24



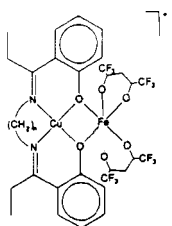
CC5 $[\text{Cu}_2(\text{L-Et})(\text{N}_3)]^{2+}$

24



CC6 $[\text{Cu}_2(\text{bpeac})(\text{N}_3)]^{2+}$

25

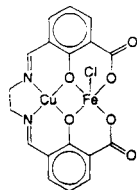


CF1 $\{\text{Cu}[(\text{prp})_2\text{en}]\text{Fe}(\text{hfa})_2\}^+ \quad (n = 2)$

26^b

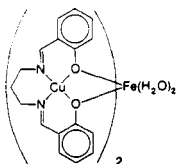
CF2 $\{\text{Cu}[(\text{prp})_2\text{pn}]\text{Fe}(\text{hfa})_2\}^+ \quad (n = 3)$

26^b



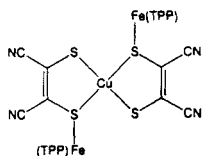
CF3 $\text{Cu}[(\text{isa})_2\text{en}]\text{FeCl}$

20



CF4 $\{[\text{Cu}(1,3\text{-prnS})]_2\text{Fe}(\text{H}_2\text{O})_2\}^{2+}$

26^b



CF5 $[(\text{TPP})\text{Fe}(\text{mnt})\text{Cu}(\text{mnt})\text{Fe}(\text{TPP})]$

27

^aReferences are to crystal structures unless otherwise noted.

^bCrystal structures have not been published.

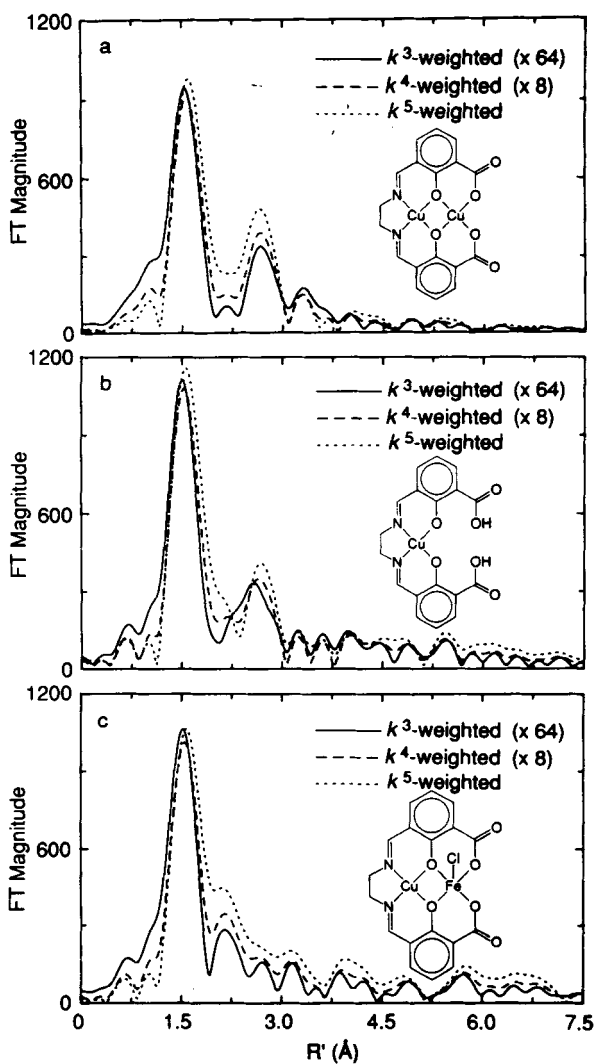


FIGURE 3 k^n -weighted FTs ($n = 3-5$, $k = 3-13 \text{ \AA}^{-1}$) of Cu EXAFS for compounds CC3 (a), C3 (b), and CF3 (c).

The height of the $R' \approx 2.7$ Å FT peak due to $\text{Cu}\cdots\text{C}$, $\text{Cu}\cdots\text{Cu}$ scattering in Fig. 3a exhibits the expected dependence on k^n weighting (i.e., the FT peak height increases with increasing n), but a somewhat similar trend is also observed for the mononuclear derivative in Fig. 3b in the absence of any $\text{Cu}\cdots\text{M}$ scattering. This type of "false positive" result is more clearly demonstrated in the k^n -weighted FTs of the mononuclear $[\text{Cu}(\text{imidH})_2\text{DAP}]^{2+}$ (C1) shown in Fig. 4a. Using the criterion of increasing FT peak height with increasing n (in k^n -weighted FTs), one would have to conclude that the $R' \approx 2.5$ Å FT peak in Fig. 4a contains some $\text{Cu}\cdots\text{M}$ contribution, when in fact none exists. The behavior of this FT peak is the result of an EXAFS backscattering amplitude envelope that maximizes at relatively high k , not because a heavy (M) scatterer is involved but because of a significant static disorder in the $\text{Cu}\cdots\text{C}$ shell. As shown in Fig. 4b, a statically disordered $\text{Cu}\cdots\text{C}$ shell does not always result in a "false positive" result. The height of the $R' \approx 2.6$ Å peak in the FT of $\{\text{Cu}[2,2'-(\text{imid})_2\text{biphenyl}]_2\}^{2+}$ (C2, Fig. 4b) is virtually independent of n , as might be expected for solely $\text{Cu}\cdots\text{C}$ scattering.

Figure 5 shows that other $\text{Cu}\cdots\text{Cu}$ binuclear compounds with $\text{Cu}\cdots\text{Cu}$ distances in the 3.0–3.2 Å range also exhibit FT peaks (at $R' \approx 2.7$ –2.8 Å) with heights that increase as n increases. For $[\text{Cu}_2(\text{L}')(\text{OH})]^{2+}$ (CC1, Fig. 5a), the interpretation is slightly confused by the presence of a FT peak at $R' \approx 2.2$ Å that also follows this trend. However, a peak at this position could not realistically contain a (nonbonded) $\text{Cu}\cdots\text{M}$ contribution, since the $\text{Cu}\cdots\text{M}$ distance would have to be ~ 2.6 Å.

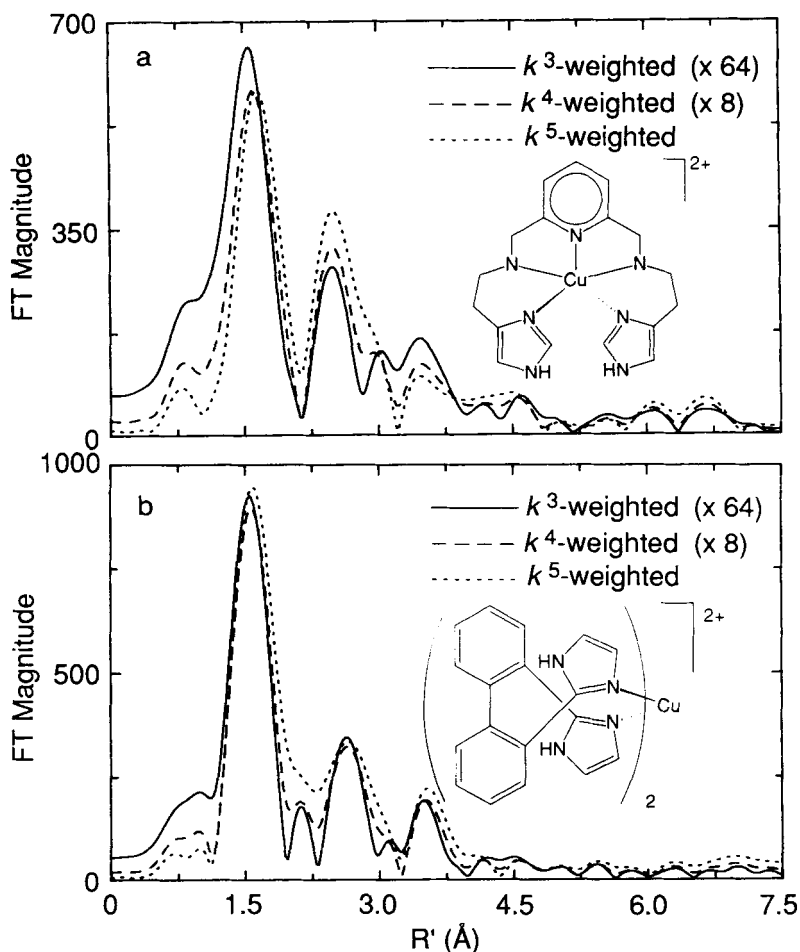


FIGURE 4 k^n -weighted FTs ($n = 3-5$, $k = 3-13 \text{ \AA}^{-1}$) of Cu EXAFS for compounds C1 (a) and C2 (b).

The closely related Cu-Fe binuclear compounds $\{\text{Cu}[(\text{prp})_2\text{en}]\text{Fe}(\text{hfa})_2\}^+$ (CF1, Fig. 7a) and $\{\text{Cu}[(\text{prp})_2\text{pn}]\text{Fe}(\text{hfa})_2\}^+$ (CF2, Fig. 7b) are expected to have Cu...Fe distances very similar to CF3 (Fig. 3c). The FTs of all three of these compounds show very little outer-shell scattering, indicating that the destructive interference of Cu...Fe and Cu...C scattering for Cu...Fe distances of $\sim 3.0 \text{ \AA}$

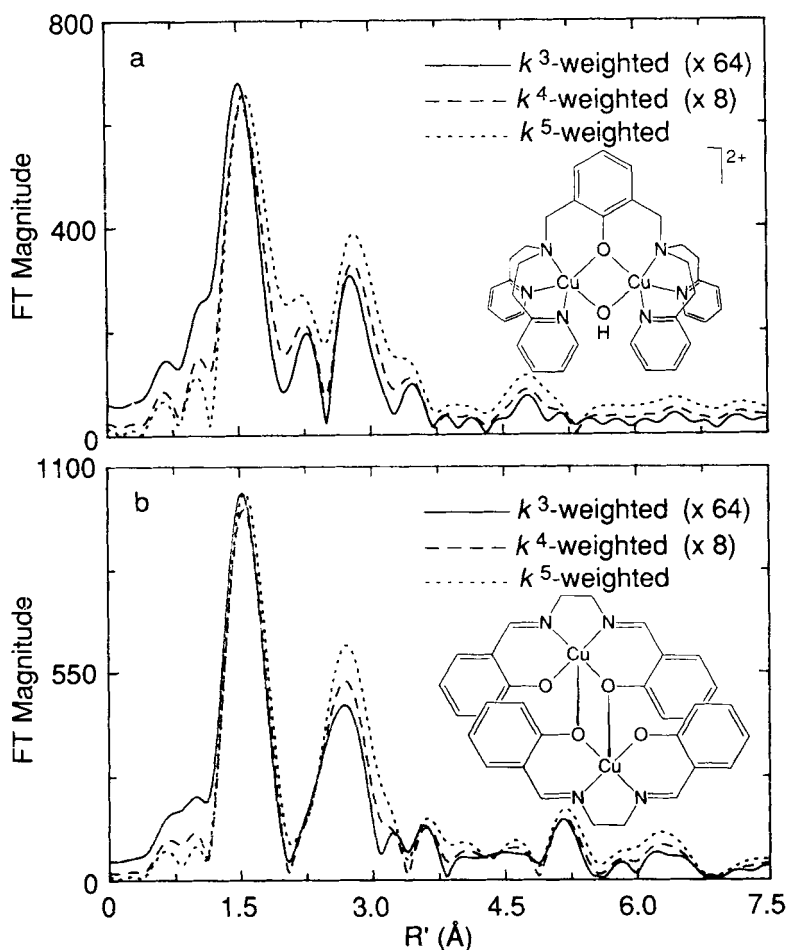


FIGURE 5 k^n -weighted FTs ($n = 3-5$, $k = 3-13 \text{ \AA}^{-1}$) of Cu EXAFS for compounds CC1 (a) and CC2 (b).

is a common phenomenon. This is contrasted by the FT of the trinuclear (Cu_2Fe) compound $\{[\text{Cu}(1,3\text{-prnS})]_2\text{Fe}(\text{H}_2\text{O})_2\}^{2+}$ (CF4, Fig. 8a), which is again expected to have a similar $\text{Cu}\cdots\text{Fe}$ distance of $\sim 3.0 \text{ \AA}$. The FTs of the Cu EXAFS of this compound exhibit peaks at $R' \approx 2.7 \text{ \AA}$, the heights of which show the expected trend with k^n weighting. Figure 8b shows the FTs for a trinuclear (CuFe_2)

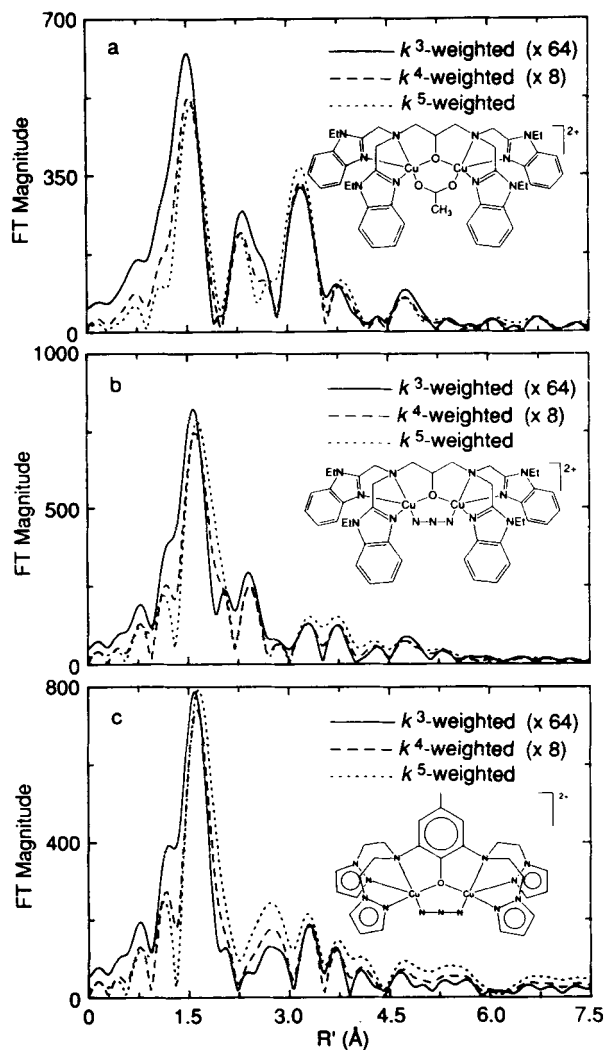


FIGURE 6 k^n -weighted FTs ($n = 3-5$, $k = 3-13 \text{ \AA}^{-1}$) of Cu EXAFS for compounds CC4 (a), CC5 (b), and CC6 (c).

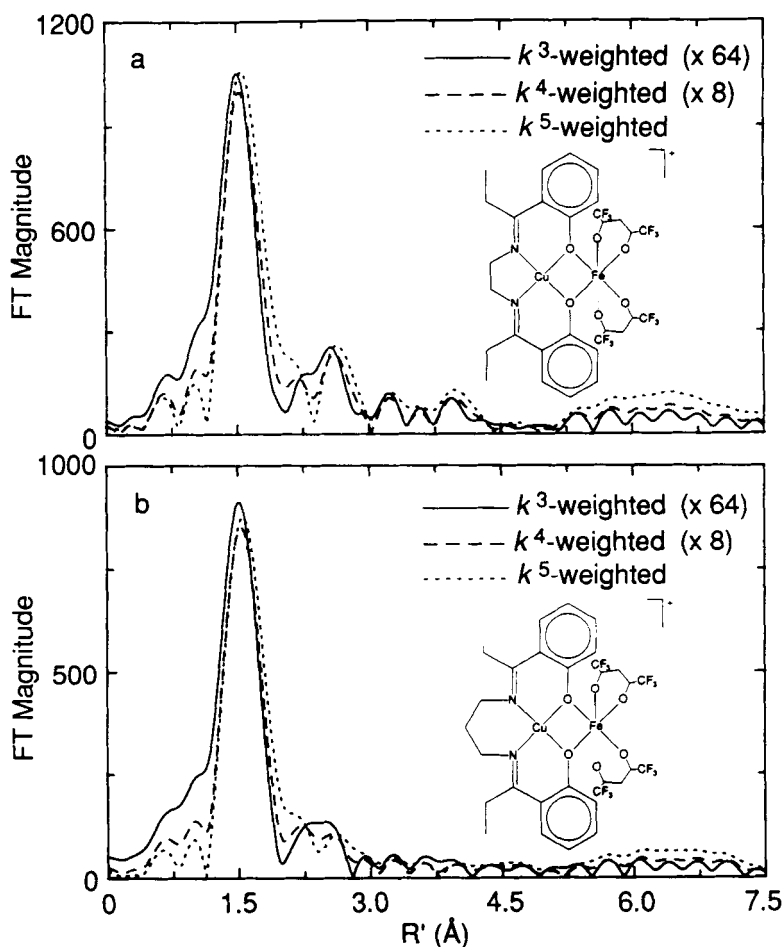


FIGURE 7 k^n -weighted FTs ($n = 3-5$, $k = 3-13 \text{ \AA}^{-1}$) of Cu EXAFS for compounds CF1 (a) and CF2 (b).

compound with a long Cu...Fe distance ($\sim 3.9 \text{ \AA}$), [(TPP)Fe(mnt)Cu(mnt)Fe(TPP)] (CF5). Although the FT peak (at $R' \approx 3.5 \text{ \AA}$ in Fig. 8b) containing the Cu...Fe scattering (in this case from two Fe scatterers) does show the expected trend with k^n weighting, so does the FT peak at $R' \approx 2.9 \text{ \AA}$.

In summary, the detection of Cu...M interactions by examina-

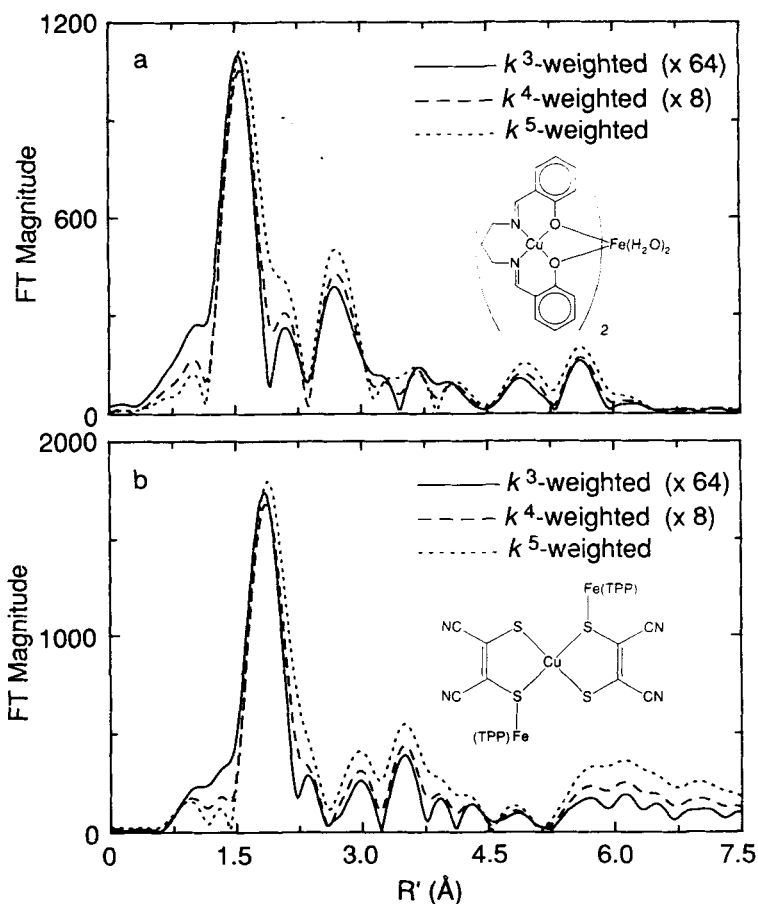


FIGURE 8 k^n -weighted FTs ($n = 3-5$, $k = 3-13 \text{ \AA}^{-1}$) of Cu EXAFS for compounds CF4 (a) and CF5 (b).

tion of the n -dependence of FT peak heights in k^n -weighted FTs does not succeed. Although the expected trends are sometimes observed, there are too many counterexamples of peak heights increasing with increasing n for FT peaks that contain no $Cu \cdots M$ interaction (e.g., C3, Fig. 3b; C1, Fig. 4a; CC6, Fig. 6c; CF5, Fig. 8b) or of $Cu \cdots M$ containing FT peaks that do not show this trend (e.g., CC5, Fig. 6b; CC6, Fig. 6c; CF1, Fig. 7a). Even more problematic is the virtual disappearance of outer-shell FT peaks in CuFe

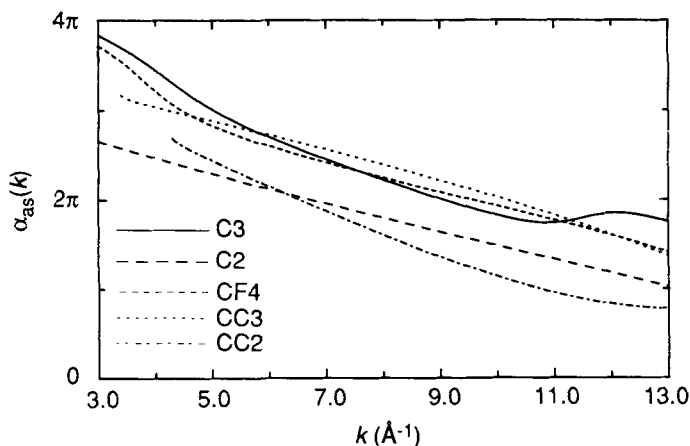


FIGURE 9 Effective backscattering phases [$\alpha_{as}(\mathbf{k})$, see Eq. (1)] extracted from outer-shell FT peaks of the indicated compounds by complex Fourier back-transformation. For each extracted shell, the position of the FT peak (R') and the distance used for the phase extraction (R_{as}) were: C3, $R' = 2.57 \text{ \AA}$, $R_{as} = 2.9 \text{ \AA}$; C2, $R' = 2.64 \text{ \AA}$, $R_{as} = 2.9 \text{ \AA}$; CF4, $R' = 2.69 \text{ \AA}$, $R_{as} = 3.0 \text{ \AA}$; CC3, $R' = 2.67 \text{ \AA}$, $R_{as} = 3.0 \text{ \AA}$; CC2, $R' = 2.69 \text{ \AA}$, $R_{as} = 3.0 \text{ \AA}$.

compounds with $R(\text{Cu}\cdots\text{Fe}) \approx 3.0 \text{ \AA}$ due to the destructive interference of $\text{Cu}\cdots\text{Fe}$ and $\text{Cu}\cdots\text{C}$ scattering (e.g., CF3, Fig. 3c; CF1, Fig. 7a; CF2, Fig. 7b).

Method 2. In order to test the possibility of using the backscattering phase as an indicator of scatterer type (i.e., $\text{Cu}\cdots\text{C}$ or $\text{Cu}\cdots\text{M}$), a representative group of Cu mononuclear and Cu-M ($\text{M} = \text{Cu}, \text{Fe}$) multinuclear compounds were compared. The effective application of this method is difficult, since it is expected to be important to compare FT peaks from different samples that fall at very similar R' (since the multiple scattering and inelastic scattering will be different for shells at different distances). Given the available data, we were able to compare phases extracted from FT peaks occurring at $R' \approx 2.7 \pm 0.1 \text{ \AA}$ (i.e., real distances of $\sim 2.9\text{--}3.1 \text{ \AA}$) and these phases [$\alpha_{as}(\mathbf{k})$, see Eq. (1)] are displayed in Fig. 9. Another technical problem with this method involves the ability to successfully extract a single FT peak. The presence of shoulders on the filtered FT peak arises from significant disorder in distances, which is reflected in beat patterns in the EXAFS. At a beat in the EXAFS, the phase goes through a (sometimes poorly resolved) disconti-

nuity, giving rise to inflection points in some of the phases plotted in Fig. 9. This makes the comparison even more difficult.

For the phase comparison method to be a viable means of identifying Cu \cdots M scattering, all the phases for FT peaks containing Cu \cdots M scattering should occur outside a tightly grouped subset of phases from FT peaks containing only Cu \cdots C scattering. Figure 9 clearly illustrates that this is not the case. The phase differences between two Cu mononuclear compounds (**C2** and **C3**) are easily as large as the differences between these and the phases from the Cu \cdots Cu (**CC2**, **CC3**) and Cu \cdots Fe (**CF4**) compounds. This type of phase comparison is apparently not a reliable method of detecting Cu \cdots M scattering.

Method 3. Since quantitative knowledge of both Cu \cdots C and Cu \cdots M backscattering functions is required for the use of curve fitting to detect Cu \cdots M interactions, the first task is to generate these functions. For this illustration, it is useful to restrict our attention to scatterers in shells ~ 3 Å from the Cu. Cu \cdots C backscattering functions can be extracted from the two structurally characterized copper mononuclear compounds, **C1** and **C2**, and can then be used to help define Cu \cdots Cu backscattering from Cu–Cu compounds that contain both Cu \cdots C and Cu \cdots Cu interactions.

Both mononuclear compounds **C1** and **C2** have two separate groups of Cu \cdots C interactions (at ~ 2.85 Å and ~ 3.1 Å) so that a series of optimizations was required to define a Cu \cdots C scale factor (B_C) and $\Delta E_0(C)$. For each compound, the FT peak at $R' \approx 2.6$ Å was Fourier-filtered (see Fig. 10a,d) and the resulting $\chi'(\mathbf{k})$ data were curve-fit using the Teo and Lee theoretical functions¹⁴ for two shells of Cu \cdots C scatterers. Coordination numbers for both shells were fixed at the crystallographic values, initial B_C and $\Delta E_0(C)$ values were guessed and kept fixed at the same value for both shells, and R_{as} , σ_{as} were optimized. A set of such optimizations were done, choosing a different B_C value each time to “manually” optimize B_C . $\Delta E_0(C)$ was then “manually” optimized by a similar set of optimizations in which $\Delta E_0(C)$ was changed and B_C was held constant at its optimized value. Performing an identical series of optimizations for both compounds resulted in best average values for B_C and $\Delta E_0(C)$ of 0.30 and +5 eV, respectively. (Recall that $E_0 = 9000$ eV was used when defining the \mathbf{k} -scale.) Fits of

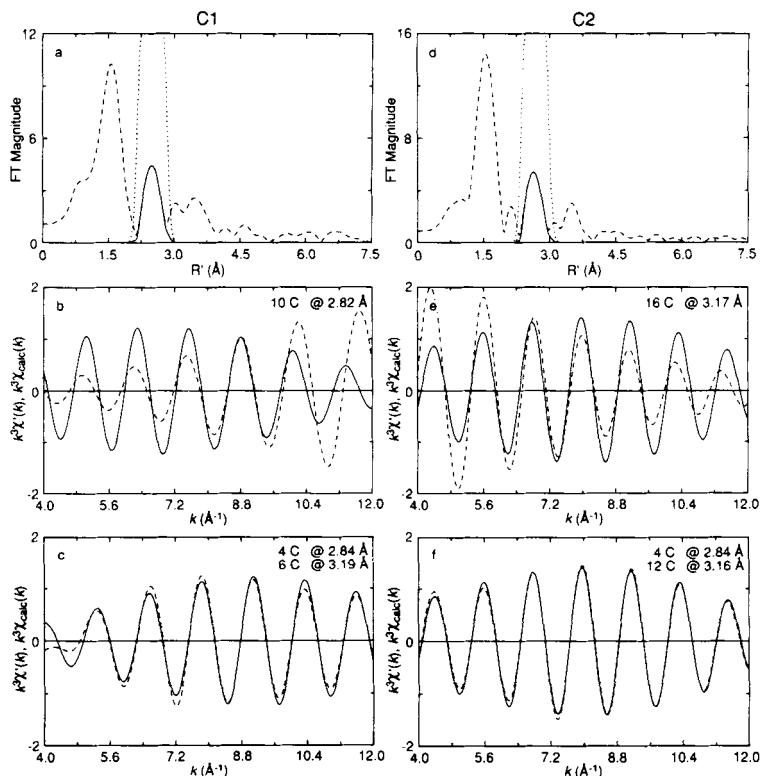


FIGURE 10 Curve-fitting results for Cu...C shells of Cu EXAFS for compounds C1 and C2. (a) k^3 -weighted FT from $k = 3\text{--}13 \text{ \AA}^{-1}$ (dashed line) and filter window (dotted line) used to generate the Cu...C shell FT data (solid line) of compound C1 which gives rise to the filtered data in (b) and (c) (solid lines). The dashed lines in (b) and (c) are simulated data from fits 2A and 2B, respectively. (d) Fourier-filtering of the Cu...C shell for compound C2 [as in (a)]. The dashed lines in (e) and (f) are simulated data from fits 2C and 2D, respectively.

the filtered $\chi'(k)$ data for compounds C1 and C2 using these values are compared in Fig. 10c,f. Figure 10b,e shows that two shells of Cu...C scatterers are required to adequately fit the data.

The numerical fit results are tabulated in Table II. The theoretical phase functions are able to reproduce the crystallographic distances within the expected accuracy ($\pm 0.02 \text{ \AA}$), except for the longer Cu...C shell of compound C1 (Fit 2B, Table II), where the

TABLE II
Curve-fitting of second-shell Cu...C interactions in structurally characterized copper mononuclear compounds

Compound	Fit	N_s	Cu...C R_{as}^a (Å)	σ_{as} (Å)	N_s	Cu...C' R_{as}^a (Å)	σ_{as} (Å)	f'^b
C1	2A	(10) ^c	2.82	0.0900	—	—	—	0.247
	2B	(4)	2.84 [2.84]	0.0000	(6)	3.19 [3.09]	0.1071	0.054
C2	2C	(16)	3.17	0.0881	—	—	—	0.173
	2D	(4)	2.84 [2.86]	0.0585	(12)	3.16 [3.15]	0.0731	0.021

^aDistances in brackets below curve-fitting results are the crystallographic averaged distances.

^b f' is a goodness-of-fit statistic normalized to the overall magnitude of the $\mathbf{k}^3\chi(\mathbf{k})$ data:

$$f' = \frac{\{\sum[\mathbf{k}^3(\chi_{\text{obsd}}(i) - \chi_{\text{calc}}(i))^2/N\}^{1/2}}{(\mathbf{k}^3\chi)_{\text{max}} - (\mathbf{k}^3\chi)_{\text{min}}}$$

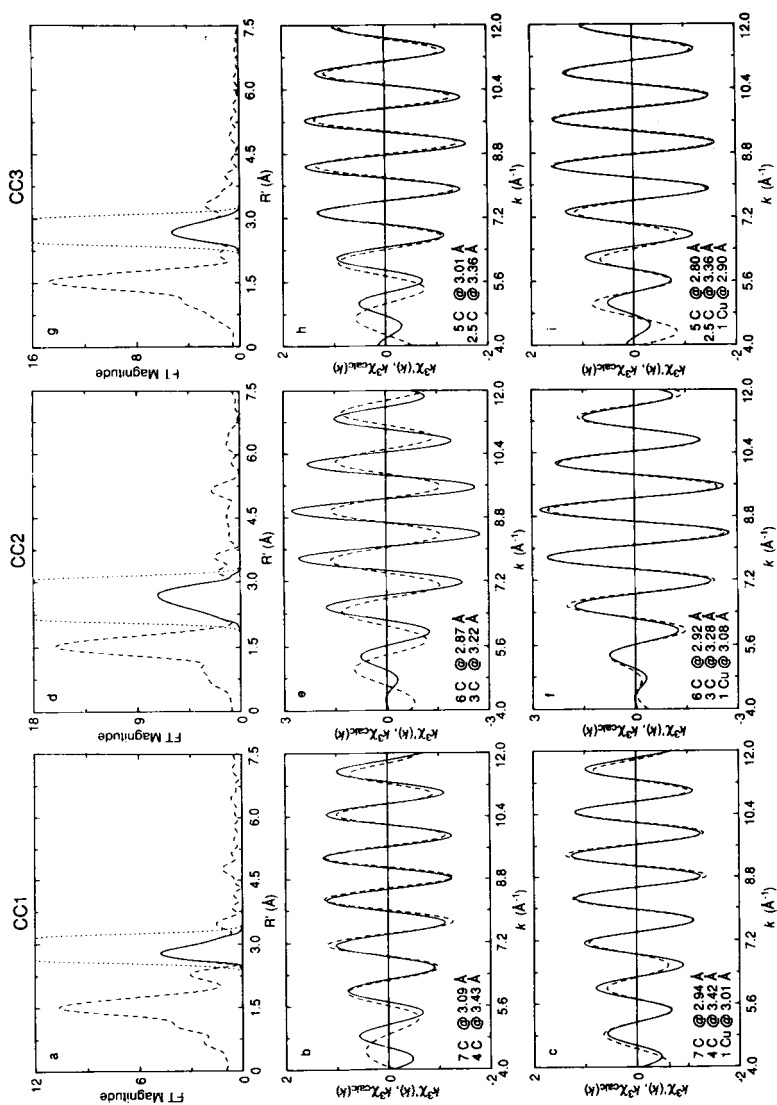
where N is the number of data points fit.

^cCoordination numbers (in parentheses) were selected as the crystallographic numbers and not varied during optimizations.

Cu...C distance is overestimated by 0.1 Å. This could be the result of our treatment ignoring multiple scattering. Also, for this optimized B_C , σ_{as} for the shorter Cu...C shell of compound **C1** (Fit 2B) is very small, indicating a structurally rigid environment. The carbons contributing to this shell are part of a 5-membered chelate metallacycle (see Table I), a structure that should not occur in biological systems. Indeed, the short Cu...C shell of compound **C2** (Fit 2D) exhibits a much less rigid environment (higher σ_{as}), as is to be expected for the much larger (and more biologically relevant) chelate ring.

For Cu...Cu scattering, the structurally characterized compounds **CC1**, **CC2**, and **CC3**, exhibiting respective Cu...Cu distances of 3.08,²¹ 3.18,²² and 2.94 Å,²³ were analyzed. In each case, at *least* two shells of Cu...C interactions also contribute to the FT peak containing the Cu...Cu scattering. The approach to determining Cu...Cu scattering functions was completely analogous to the approach described above for Cu...C, the scale factor (B_{Cu}) and $\Delta E_0(Cu)$ being manually optimized individually in curve fits that used $B_C = 0.30$ and $\Delta E_0(C) = +5$ eV for the Cu...C shells, while allowing R_{as} and σ_{as} to vary for *all* shells. The curve-fitting results summarized in Table III yield optimized values of $B_{Cu} = 1.0$ and $\Delta E_0(C) = +20$ eV. Figure 11 shows the Fourier filtering for these three compounds (Fig. 11a,d,g) as well as the best curve fits using these optimized parameters (Fig. 11c for **CC1**, 11f for **CC2**, and 11i for **CC3**).

This application of the FABM method^{16,17} for outer-shell Cu...C and Cu...Cu interactions results in EXAFS-determined distances that are sometimes different from the crystallographically determined ones. For the shorter Cu...C interactions (~ 2.8 – 2.9 Å), the distances are underestimated by an average of 0.03 Å, whereas longer Cu...C distances (~ 3.1 – 3.3 Å) are *overestimated* by an average of 0.08 Å (see Tables II and III). Cu...Cu distances near 3 Å are underestimated by an average of 0.07 Å, with the underestimation becoming more pronounced at longer distances (cf. fits 3E and 3G). For Cu...C interactions, part of the reason for these systematic errors may be our simplified arrangement of a very disordered set of Cu...C interactions into two discrete subshells (i.e., the pairwise distribution functions within these subshells are decidedly non-Gaussian); but for both Cu...C and Cu...Cu inter-



actions at this distance, the existence of a number of multiple scattering pathways which have been ignored in our treatment could be responsible for the observed discrepancies.

For each copper binuclear compound, the crystallographically established Cu...C distribution cannot adequately simulate the filtered EXAFS data in the absence of the Cu...Cu contribution. The goodness-of-fit index f' improves by a factor ranging from 1.5–3.8 upon addition of a Cu...Cu shell to two Cu...C shells (cf. fits 3B and 3A for CC1, 3F and 3E for CC2, 3H and 3G for CC3). However, since we wish to use these Cu...Cu scattering functions on Cu EXAFS data from enzymes with undetermined structures, we cannot assume that we know the distribution (or even the number) of Cu...C interactions. Unfortunately, given an alternate arrangement of C's about Cu, the data for compound CC1 can readily be simulated by three separate shells of Cu...C and *no* Cu...Cu interactions (fit 3C). Also for this compound, the Cu...C and Cu...Cu distances determined in the correct simulation (fit 3A) are *not* uniquely determined. Given the same numbers of Cu...C and Cu...Cu interactions, an alternate set of distances can also provide a good simulation of the data (fit 3D). Thus, one must be careful with multiple-shell curve fitting to examine all possible combinations of interactions to identify those that give adequate simulations. Often no *unique* structural solution exists, which in the cases discussed here results in an inability to determine the existence of a Cu...M interaction.

Therefore, whether this curve-fitting method can be used to detect the presence of Cu...M interactions depends on the data set being examined. If one can adequately simulate the outer-shell scattering by inclusion of a Cu...M interaction and no other physically reasonable arrangement of C scatterers alone can do as well, only then has a Cu...M interaction been detected. In many cases, the only conclusion may be that the presence of a Cu...M interaction is one of a number of acceptable structural solutions.

FIGURE 11 Curve-fitting results for Cu...Cu, Cu...C shells of Cu EXAFS for compounds CC1, CC2, and CC3. (a) Fourier-filtering of the Cu...Cu, Cu...C shell for compound CC1 (see caption for Fig. 10a). The dashed lines in (b) and (c) are simulated data from fits 3B and 3A, respectively. (d) Fourier-filtering of the Cu...Cu, Cu...C shell for compound CC2. The dashed lines in (e) and (f) are simulated data from fits 3F and 3E, respectively. (g) Fourier-filtering of the Cu...Cu, Cu...C shell for compound CC3. The dashed lines in (h) and (i) are simulated data from fits 3H and 3G, respectively.

TABLE III
Curve-fitting of second-shell Cu...C + Cu...Cu interactions in structurally characterized copper binuclear compounds

Compound	Fit	N_s	Cu...C R_{as}^a (Å)	σ_{as} (Å)	N_s	Cu...Cu R_{as}^a (Å)	σ_{as} (Å)	f^{1b}
CC1	3A	(7) ^c	2.94 [2.94]	0.0770	(1)	3.01 [3.08]	0.0860	0.051
		(4)	3.42 [3.20]	0.0021				
	3B	(7)	3.09 [3.43]	0.0672 0.0000	–	–	–	0.108
		(4)	3.43					
	3C	(2)	2.85 [3.09]	0.0635 0.0292	–	–	–	0.036
CC2	3D	(5)	3.09					
		(4)	3.44 [3.24]	0.0249 0.1292	(1)	3.33	0.0743	0.051
	3E	(7)	3.24					
		(4)	3.62 [2.92]	0.0506 0.0485	(1)	3.08 [3.18]	0.0700	0.027
	(6)	2.92 [2.96]						
CC3	3F	(3)	3.28 [3.29]	0.0000				
		(6)	2.87	0.0002	–	–	–	0.104
	3G	(3)	3.22 [2.80]	0.0000				
		(5)	2.80 [2.89]	0.0000	(1)	2.90 [2.94]	0.0723	0.065
	3H	(2.5)	3.36 [3.28]	0.0000				
(5)		3.01	0.0000	–	–	–	0.096	
		(2.5)	3.36	0.0000				

^aDistances in brackets below curve-fitting results are the crystallographic averaged distances.

^b f^b is defined as in Table II.

^cCoordination numbers (in parentheses) were selected as the crystallographic numbers and not varied during optimizations.

Application to Copper Enzymes. EPR spectra of dopamine β -hydroxylase (DBH) in its oxidized [Cu(II)] state are typical of mononuclear type 2 Cu(II).^{28–32} However, the catalytic reaction (conversion of dopamine to norepinephrine) requires reduction of DBH to Cu(I) and the kinetics suggest the possibility of a binuclear site in the Cu(I) form.³³ Our Cu EXAFS data on the ascorbate-reduced enzyme collected at 10 K³⁴ give rise to FT peaks in the positions expected for Cu...C scattering arising from histidine imidazole ligation (see Fig. 12a). We can use the curve-fitting pro-

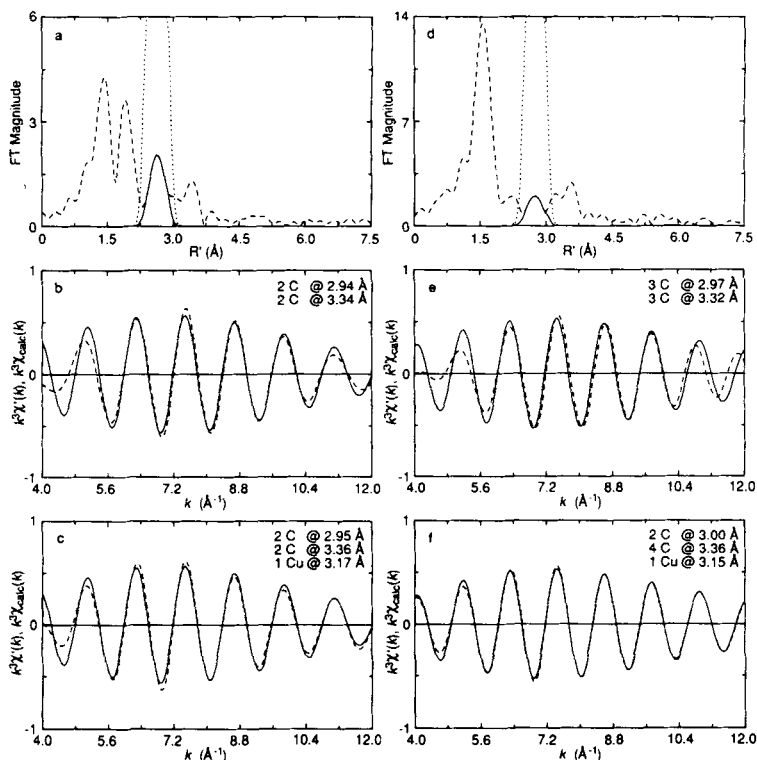


FIGURE 12 Curve-fitting results for outer shells of Cu EXAFS for the reduced (a, b, c) and oxidized (d, e, f) forms of dopamine β -hydroxylase (DBH). (a) Fourier-filtering of the outer shell for reduced [Cu(I)] DBH (see caption for Fig. 10a). The dashed lines in (b) and (c) are simulated data from fits 4A and 4C, respectively. (d) Fourier-filtering of the outer shell for oxidized [Cu(II)] DBH. The dashed lines in (e) and (f) are simulated data from fits 4D and 4E, respectively.

cedure described above to test for the presence of Cu...Cu scattering in the FT peak at $R' \approx 2.6 \text{ \AA}$ (Fig. 12a).

The results of curve fitting of the Fourier-filtered EXAFS data from extraction of this FT peak (shown as solid lines in Fig. 12b,c) are summarized in Table IV. In these fits, we have assumed the presence of two imidazoles bound to the Cu(I), consistent with our analysis of the first-shell data and the edge spectrum.³⁴ Assuming a static disorder in imidazole ligation (e.g., tilting of the imidazoles) allows a reasonable fit of the filtered data with two sets of Cu...C distances and no Cu...Cu scattering (Fit 4A, Fig. 12b). Fit 4B shows that a single Cu...Cu shell in the absence of any Cu...C scattering can fit the data almost as well. This points out the folly of comparing only goodness-of-fit (f') values, since the presence of the FT peak at $R' \approx 3.4 \text{ \AA}$ (Fig. 12a) confirms the presence of imidazoles which *must* then contribute some Cu...C scattering to the $R' \approx 2.6 \text{ \AA}$ FT peak. Also, using f' as a guide, fit 4C would be considered the best, indicating the presence of Cu...Cu scattering with two shells of Cu...C scattering. However, the Debye-Waller σ_{as} for the Cu...Cu shell of this fit is very large compared to values seen for structurally characterized models (see Table III), making this a physically unreasonable structure.

Thus, for ascorbate-reduced DBH, we conclude that there is probably not a Cu...Cu interaction around 3.2 \AA , unless it is a very weak interaction (giving rise to the large σ_{as} in fit 4C). Very few structurally characterized Cu(I)...Cu(I) binuclear compounds with short Cu(I)...Cu(I) distances are available to determine whether this large σ_{as} is reasonable or not.

It is instructive to compare these results with the results for the oxidized form of DBH, the Cu EXAFS FT of which also shows a peak at $R' \approx 2.7 \text{ \AA}$ of about the same magnitude (Fig. 12d; note the difference in scales on the ordinates of Fig. 12a,d). As already mentioned, oxidized DBH with two coppers per subunit exhibits a type 2 EPR signal, the quantitation of which accounts for all of the coppers.²⁸⁻³² Thus, it is extremely unlikely that a binuclear site with a Cu...Cu distance of $\sim 3\text{--}3.5 \text{ \AA}$ occurs in this derivative. Assuming three imidazoles per copper,³⁴ one can obtain a barely adequate fit assuming two shells of Cu...C interactions (fit 4D). Adding a Cu...Cu shell improves f' by more than a factor of 4, although a fairly large σ_{as} for the Cu...Cu shell and an uneven

TABLE IV
Curve-fitting of second-shell interactions in the copper-containing enzyme dopamine β -hydroxylase

Enzyme	Fit	N_s	$\text{Cu}\cdots\text{C}$ $R_{\text{as}} (\text{\AA})$	$\sigma_{\text{as}} (\text{\AA})$	N_s	$\text{Cu}\cdots\text{Cu}$ $R_{\text{as}} (\text{\AA})$	$\sigma_{\text{as}} (\text{\AA})$	f'^a
DBH, ascorbate-reduced	4A	(2) ^b	2.94	0.0362	—	—	—	0.089
		(2)	3.34	0.0549				
	4B	—	—	—	(1)	3.22	0.1222	0.125
	4C	(2)	2.95	0.0369	(1)	3.17	0.1608	0.058
DBH, oxidized		(2)	3.36	0.0847				
	4D	(3)	2.97	0.0936	—	—	—	0.111
		(3)	3.32	0.0538				
	4E	(2)	3.00	0.0360	(1)	3.15	0.1488	0.023
		(4)	3.36	0.1007				
	4F	(2)	2.98	0.0683	—	—	—	0.048
		(2)	3.28	0.0000				
		(2)	3.40	0.0378				

^a f' is defined as in Table II.

^bCoordination numbers (in parentheses) were not varied during optimizations.

distribution of Cu...C interactions are required (fit 4E). Some, but not all, of this improvement can be explained simply by the increase in the degrees of freedom, since a fit with three separate Cu...C (and no Cu...Cu) shells (fit 4F) is significantly better than the two Cu...C shell fit (4D).

The structural results from the Cu...Cu, Cu...C fits for the oxidized and reduced forms of DBH are strikingly similar (cf. fits 4C, 4E). Since it is clear from EPR that a Cu...Cu distance of 3.15 Å in oxidized DBH is virtually impossible, the curve-fitting results of fit 4E must be artifactual. If this is true, then the presence of a Cu...Cu component in fit 4C could also be an artifact, suggesting that the EXAFS curve fitting provides no real evidence for a Cu...Cu interaction in reduced DBH.

It is somewhat disturbing to note that in the absence of any independent knowledge about the copper site structure in oxidized DBH, the Cu EXAFS curve-fitting results (fits 4C, 4E) could easily have been interpreted as indicating a Cu...Cu separation of ~3.2 Å in both oxidized and reduced forms of DBH. (The large σ_{as} values could be rationalized as due to microheterogeneity or to a binuclear structure considerably less rigid than the doubly-bridged model compounds examined herein.) It is very unlikely that this is the case. We are forced to conclude that this curve-fitting approach is not only subject to "false negative" results (not identifying a Cu...Cu interaction known to be present—fit 3C) but also to "false positive" results (detecting a Cu...Cu interaction when none exists—fit 4E).

CONCLUSIONS

The purpose of this exercise was to discover not the failures but the limitations of the EXAFS technique in sensing longer distance scattering atoms. It should be reemphasized that the problems encountered are not due to an inherent flaw in the EXAFS technique, but arise because of the complexity of the highly unsymmetrical structural environment typically found in biological metal sites. Thus, the overlapping of a large number of scattering contributions from different atoms at slightly different distances results in an inability to identify a unique structural solution using EXAFS

curve-fitting techniques. This overlapping of scattering contributions apparently also sufficiently alters the effective backscattering amplitude envelope and phase derived from the composite FT peak so that amplitude envelope and phase comparisons (Methods 1 and 2, *vide supra*) also fail to uniquely identify the presence of a metal scatterer.

The curve-fitting approach described here relies on Fourier filtering of the Cu EXAFS data to isolate the scattering components of interest (i.e., the scattering components in a limited R' range of the FT). It must be remembered that such an isolation procedure does not necessarily yield all the scattering components in a similarly limited R range (i.e., in a real distance range). FT peaks cannot be completely separated from neighboring peaks due to overlap. Perhaps more importantly, since the FT's used for the filtering process were derived from $k^3\chi(k)$ data, the FT peaks appear more resolved (due to the artificial resolution enhancement of the k^3 weighting function) than they really are. Thus, a given peak in a k^3 -weighted FT does not necessarily reflect a true "shell" of scattering atoms. The filtering process may then distort the scattering components by selecting out the smaller R' range suggested by the resolution-enhanced FT peak. The usual justification for using this Fourier-filtering procedure is that the curve fitting uses scattering functions that are derived from similar filters of similar k^3 -weighted FTs of "model" compound EXAFS data. This *may* compensate for the distortion of the scattering components for shorter distances ("first-shell") scatterers, but for very disordered outer shells, the *different* distribution of scattering components in the "model" compared to the "unknown" makes appropriate compensation extremely unlikely (unless the "model" compound structure is very similar to the "unknown" structure).

A potential solution to this problem is to perform the curve fitting on raw (unfiltered) EXAFS data. Unfortunately, even given appropriate scattering functions, for the type of structures examined herein, simulation of the raw EXAFS would require about six shells of scatterers. Since the fits we describe on Fourier-filtered data were often equally good with and without a Cu...M component, one would certainly expect no significant change in the quality (f') of a fit in which most of the EXAFS is contributed by first-shell scatterers. In other words, the underlying difficulty in de-

tecting Cu...M scattering in the cases we have described is the small overall contribution of the Cu...M scattering to the EXAFS, as well as the ability of other potential scatterers to mimic (replace) the Cu...M scattering component in the simulation.

Our results suggest that identification of M...M scattering at ≥ 3 Å in metallobiomolecules is fraught with difficulties and ambiguity. It is possible that better scattering functions or treatment of multiple scattering effects will improve the situation, but it should be realized that evidence for EXAFS simulations being *unique* should always be a required part of a structural determination, particularly when dealing with outer-shell scatterers.

Acknowledgments

The following people are gratefully acknowledged for providing samples of the indicated compounds: C1, L. J. Wilson; C2, H. J. Schugar; CC1, CC4, CC5, CC6, R. E. Dolle and L. I. Kruse; CC2, I. Morgenstern-Badarau; CF1, CF2, CF4, E. Sinn; CF5, C. M. Elliott. Dr. J. R. Schwartz is acknowledged for the synthesis of samples of compounds C3, CC3, and CF3. The x-ray absorption measurements were performed at the Stanford Synchrotron Radiation Laboratory (SSRL), which is supported by the Department of Energy, Office of Basic Energy Sciences, and the National Institutes of Health, Biotechnology Resource Program, Division of Research Resources. XAS work under R.A.S. is supported by the National Science Foundation (DMB 86-45819). R.A.S. is a NSF Presidential Young Investigator and an Alfred P. Sloan Research Fellow.

References

1. R. A. Scott, *Methods Enzymol.* **117**, 414 (1985).
2. S. P. Cramer, In *X-Ray Absorption Principles, Applications, Techniques of EXAFS, SEXAFS, and XANES*, eds. D. C. Koningsberger and R. Prins, (John Wiley & Sons, New York, 1988), p. 257.
3. S. S. Hasnain, *Life Chemistry Reports* **4**, 273 (1987).
4. R. G. Shulman, P. Eisenberger and B. M. Kincaid, *Ann. Rev. Biophys. Bioeng.* **7**, 559 (1978).
5. W. T. Elam, E. A. Stern, J. D. McCallum and J. Sanders-Loehr, *J. Am. Chem. Soc.* **105**, 1919 (1983).
6. W. A. Hendrickson, M. S. Co, J. L. Smith, K. O. Hodgson and G. L. Klippenstein, *Proc. Natl. Acad. Sci. USA* **79**, 6255 (1982).
7. R. C. Scarrow, M. J. Maroney, S. M. Palmer, L. Que, Jr., A. L. Roe, S. P. Salowe and J. Stubbe, *J. Am. Chem. Soc.* **109**, 7857 (1987).
8. G. L. Woolery, L. Powers, M. Winkler, E. I. Solomon and T. G. Spiro, *J. Am. Chem. Soc.* **106**, 86 (1984).
9. M. S. Co and K. O. Hodgson, *J. Am. Chem. Soc.* **103**, 3200 (1981).

10. M. S. Co, K. O. Hodgson, T. K. Eccles and R. Lontie, *J. Am. Chem. Soc.* **103**, 984 (1981).
11. W. P. J. Gaykema, W. G. J. Hol, J. M. Vereijken, N. M. Soeter, H. J. Bak and J. J. Beintema, *Nature* **309**, 23 (1984); B. Linzen, N. M. Soeter, A. F. Riggs, H.-J. Schneider, W. Schartau, M. D. Moore, E. Yokota, P. Q. Behrens, H. Nakashima, T. Takagi, T. Nemoto, J. M. Vereijken, H. J. Bak, J. J. Beintema, A. Volbeda, W. P. J. Gaykema and W. G. J. Hol, *Science* **229**, 519 (1985); W. P. J. Gaykema, A. Volbeda and W. G. J. Hol, *J. Mol. Biol.* **187**, 255 (1985).
12. R. A. Scott, J. R. Schwartz and S. P. Cramer, *Biochemistry* **25**, 5546 (1986).
13. L. Powers, B. Chance, Y. Ching and P. Angiolillo, *Biophys. J.* **34**, 465 (1981).
14. B.-K. Teo and P. A. Lee, *J. Am. Chem. Soc.* **101**, 2815 (1979).
15. P. A. Lee, P. H. Citrin, P. Eisenberger and B. M. Kincaid, *Rev. Mod. Phys.* **53**, 769 (1981).
16. B.-K. Teo, M. R. Antonio, D. Coucouvanis, E. D. Simhon and P. P. Stremple, *J. Am. Chem. Soc.* **105**, 5767 (1983).
17. B.-K. Teo, in *EXAFS: Basic Principles and Data Analysis* (Springer-Verlag, Berlin, 1986).
18. J. D. Korp, I. Bernal, C. L. Merrill and L. J. Wilson, *J. Chem. Soc., Dalton*, 1951 (1981).
19. S. Knapp, T. P. Keenan, X. Zhang, R. Fikar, J. A. Potenza and H. J. Schugar, *J. Am. Chem. Soc.* **109**, 1882 (1987).
20. Y. Journaux, O. Kahn, J. Zarembowitch, J. Galy and J. Jaud, *J. Am. Chem. Soc.* **105**, 7585 (1983).
21. K. D. Karlin, J. C. Hayes, Y. Gultneh, R. W. Cruse, J. W. McKown, J. P. Hutchinson and J. Zubieta, *J. Am. Chem. Soc.* **106**, 2121 (1984).
22. D. Hall and T. N. Waters, *J. Chem. Soc.*, 2644 (1960).
23. O. Kahn, J. Galy, Y. Journaux, J. Jaud and I. Morgenstern-Badarau, *J. Am. Chem. Soc.* **104**, 2165 (1982).
24. V. McKee, M. Zvagulis, J. V. Dagdigian, M. G. Patch and C. A. Reed, *J. Am. Chem. Soc.* **106**, 4765 (1984).
25. T. N. Sorrell, C. J. O'Connor, O. P. Anderson and J. H. Reibenspies, *J. Am. Chem. Soc.* **107**, 4199 (1985).
26. This compound was generously donated by Professor Ekk Sinn, University of Virginia.
27. C. K. Schauer, K. Akabori, C. M. Elliott and O. P. Anderson, *J. Am. Chem. Soc.* **106**, 1127 (1984).
28. W. E. Blumberg, M. Goldstein, E. Lauber and J. Peisach, *Biochim. Biophys. Acta* **99**, 187 (1965).
29. S. Friedman and S. Kaufman, *J. Biol. Chem.* **241**, 2256 (1966).
30. G. A. Walker, H. Kon and W. Lovenberg, *Biochim. Biophys. Acta* **482**, 309 (1977).
31. T. Skotland, L. Petersson, D. Bäckström, T. Ljones, T. Flatmark and A. Ehrenberg, *Eur. J. Biochem.* **103**, 5 (1980).
32. D. E. Ash, N. J. Papadopoulos, G. Colombo and J. J. Villafranca, *J. Biol. Chem.* **259**, 3395 (1984).
33. L. I. Kruse, W. E. DeWolf, Jr., P. A. Chambers and P. J. Goodhart, *Biochemistry* **25**, 7271 (1986).
34. R. A. Scott, R. J. Sullivan, W. E. DeWolf, Jr., R. E. Dolle and L. I. Kruse, *Biochemistry* (in press).